Solid-State Electronics 186 (2021) 108103

Contents lists available at ScienceDirect

Solid State Electronics

journal homepage: www.elsevier.com/locate/sse

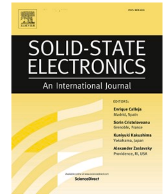

Coupled spin and charge drift-diffusion approach applied to magnetic tunnel junctions

S. Fiorentini [a,*], J. Ender [a], S. Selberherr [b], R.L. de Orio [b], W. Goes [c], V. Sverdlov [a]

[a] Christian Doppler Laboratory for Nonvolatile Magnetoresistive Memory and Logic at the Institute for Microelectronics, Austria
[b] Institute for Microelectronics, TU Wien, Gußhausstraße 27–29/E360, 1040 Vienna, Austria
[c] Silvaco Europe Ltd., Cambridge, United Kingdom

ARTICLE INFO

The review of this paper was arranged by Bogdan Cretu

Keywords:
Spin and charge drift-diffusion
Spin-transfer torque
Magnetic tunnel junctions
STT-MRAM

ABSTRACT

A drift-diffusion approach to coupled spin and charge transport has been commonly applied to determine the spin-transfer torque acting on the magnetization in metallic valves. This approach, however, is not suitable to describe the predominant tunnel transport in magnetic tunnel junctions. In this work we present a coupled Finite Element solution to the spin and charge drift–diffusion equations. We demonstrate that by introducing a magnetization dependent resistivity one can successfully reproduce the resistance dependence on the magnetization orientation in the ferromagnetic layers. We then investigate the dependence of the resulting torques on system parameters, and show that the approach is able to reproduce the torque magnitude expected in a magnetic tunnel junction. As a unique set of equations is used for the entire structure, this constitutes an efficient Finite Element based approach to describe the magnetization dynamics in emerging spin-transfer torque memories.

1. Introduction

In recent years, the outstanding improvements in the development of computer memories has been possible thanks to the scaling of semiconductor devices. This, however, has increased stand-by power consumption of traditional volatile components, such as SRAM and DRAM, due to the presence of leakage currents [1]. Nonvolatile flash memories are also becoming increasingly complex and expensive to downscale for embedded application [2]. Moreover, the price for a gigabit of traditional memories does not follow the technology node as it ceased to decrease. It prompts emerging memories entering the market to replace NOR flash, SRAM, and DRAM for stand-alone and embedded applications. Emerging memories must be nonvolatile to avoid leakages. Spin-transfer torque magnetoresistive RAM (STT-MRAM) is a nonvolatile memory which possesses a simple structure and is compatible with CMOS technology. In contrast to flash memory, STT-MRAM is fast and has a high endurance. This makes it particularly suitable for both, stand-alone as well as embedded applications, for example, in Systems-on-Chip, where STT-MRAM is poised to replace SRAM and flash memories [3–8].

The binary information in modern magnetic memories is stored in the magnetic layers of a magnetic tunnel junction (MTJ), cf. Fig. 1, where non-magnetic contacts (NM) are included. When the magnetization vectors are in a parallel state (P), the resistance is lower than in the anti-parallel state (AP). The switching between these two stable configurations can be achieved by an electric current passing through the structure. The electrons flowing through the fixed reference layer (RL) become spin-polarized, generating a spin current. When entering the free layer (FL), the spin current acts on the magnetization via the exchange interaction. As the total spin angular momentum must be preserved, if the magnetization in the layers is not aligned, the polarization is quickly absorbed, generating the spin-transfer torque [9]. If the current is sufficiently strong, the magnetization of the free layer can be switched between the two stable configurations, parallel or anti-parallel, relative to the reference layer.

Modeling of STT switching, which allows to describe the writing process of an STT-MRAM cell, requires a solution of the time-dependent Landau-Lifshitz-Gilbert (LLG) equation with the inclusion of a term describing the torque acting on the magnetization. Such a task can be performed by assuming a Slonczewski-like torque approach [10]. This, however, allows to approximately simulate the magnetization dynamics of the free layer only. A more complete description of the process can be obtained by computing the non-equilibrium spin accumulation across the whole structure. In a spin-valve structure with a non-magnetic

* Corresponding author.
E-mail address: fiorentini@iue.tuwien.ac.at (S. Fiorentini).

https://doi.org/10.1016/j.sse.2021.108103
Received 6 December 2020; Received in revised form 20 May 2021; Accepted 27 May 2021
Available online 2 June 2021
0038-1101/© 2021 Elsevier Ltd. All rights reserved.

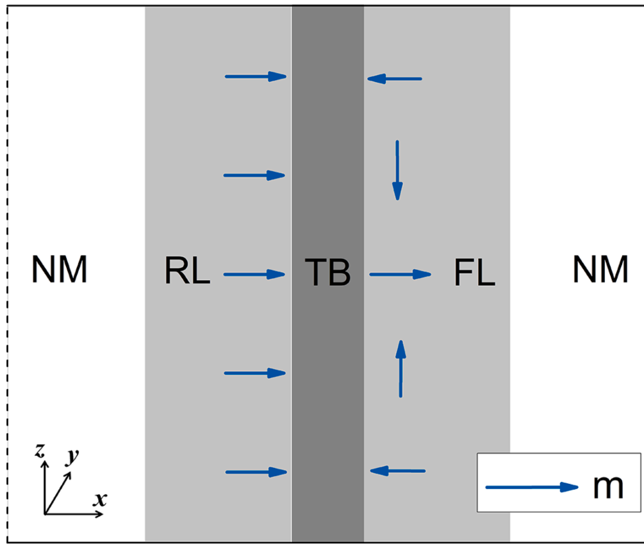

Fig. 1. MTJ structure with non-uniform magnetization configuration. The structure is composed of a reference layer (RL), a tunnel barrier (TB), a free layer (FL), and two non-magnetic contacts (NM).

spacer layer, this has been successfully accomplished by solving the spin and charge drift–diffusion equations [11,12]. Modern STT-MRAM cells, however, employ a Magnetic Tunnel Junction (MTJ) for the memory bit. In this paper we focus on the computation of the torque based on the drift–diffusion formalism. We employ an Open Source Finite Element (FE) library [13] to solve the spin and charge drift–diffusion equations. The implementation is tested against known analytical results. We then propose a method to apply these equations to an MTJ. The resistance of the oxide layer defines the current through an MTJ, as it is much larger than the resistances of the ferromagnetic layers. The main feature observed in MTJs is the strong dependence of the resistance on the relative orientation of the magnetization vectors in the RL and FL, which can also vary with the position along the interface. In order to reproduce these properties, we model the oxide layer as a (poor) conductor whose (large) resistivity depends on the relative orientation of the magnetization to obtain the current density. The current can then be used to compute the spin accumulation and extract the torque acting on the magnetization. Knowing the torque in all ferromagnetic layers opens up the possibility of including it in the LLG equation to perform simulations of the writing process in STT-MRAM and describe the switching behavior in complex multi-layered structures. This paper represents an extension of results previously presented in [14].

2. STT-MRAM

The key element in modern MRAM cells is the MTJ. It is composed of a sandwich of two ferromagnetic layers, usually made of CoFeB, and an oxide layer, usually MgO. The MTJ is characterized by the tunneling magnetoresistance ratio (TMR), defined as

$$TMR = \frac{G_P - G_{AP}}{G_{AP}}, \tag{1}$$

where G_P (G_{AP}) is the conductance in the P (AP) state. A high TMR is important to be able to distinguish between the two different configurations. Modern devices can reach a ratio of about 200% and higher [15]. Thin layers of CoFeB on MgO are perpendicularly magnetized, due to the interface-induced perpendicular anisotropy. The switching currents in a perpendicularly magnetized structure are lower than the ones in structures with in-plane magnetization, as the current-driven and thermally assisted switching go over the same energy barrier. The magnetization in the so-called free layer can switch, while the magnetization in the so-called reference layer is fixed, usually by antiferromagnetic exchange coupling to a pinned layer [16].

Accurate simulation of STT-MRAM demands a solution of the Landau-Lifshitz-Gilbert (LLG) equation describing the unit vector magnetization $\mathbf{m}$, defined as $\mathbf{M}/M_S$, where $\mathbf{M}$ is the magnetization and M_S is the saturation magnetization, subject to the spin-transfer torque. The equation reads

$$\frac{\partial \mathbf{m}}{\partial t} = -\gamma\mu_0 \mathbf{m} \times \mathbf{H}_{\text{eff}} + \alpha \mathbf{m} \times \frac{\partial \mathbf{m}}{\partial t} + \frac{1}{M_S}\mathbf{T}_\mathbf{S}, \tag{2}$$

where γ is the gyromagnetic ratio, μ_0 is the magnetic permeability, α is the Gilbert damping constant, M_S is the saturation magnetization, and $\mathbf{H}_{\text{eff}}$ includes various contributions, mainly the external field, the exchange interaction, and the demagnetizing field. In order to predict the magnetization behavior during switching, it is necessary to properly compute the STT term, $\mathbf{T}_\mathbf{S}$. This torque is generated by a non-equilibrium spin accumulation $\mathbf{S}$ acting on the magnetization via the exchange interaction and can be expressed as [12]

$$\mathbf{T}_\mathbf{S} = -\frac{D_e}{\lambda_J^2}\mathbf{m} \times \mathbf{S} - \frac{D_e}{\lambda_\varphi^2}\mathbf{m} \times (\mathbf{m} \times \mathbf{S}), \tag{3}$$

where λ_J is the spin exchange length, λ_φ is the spin dephasing length, and D_e is the electron diffusion constant. $\mathbf{S}$ is created when an electric current passes through the structure and gets polarized by the magnetic layers. In order to obtain $\mathbf{S}$, the coupled spin and charge transport must be solved.

3. Spin drift-diffusion

The drift–diffusion equations for spin current and spin accumulation are [11,12,18]

$$\overline{\mathbf{J}_\mathbf{S}} = \frac{\mu_B}{e}\beta_\sigma \mathbf{m} \otimes \left(\mathbf{J}_\mathbf{C} + \beta_D D_e \frac{e}{\mu_B}\left[(\nabla\mathbf{S})^T\mathbf{m}\right]\right) - D_e \nabla\mathbf{S}, \tag{4a}$$

$$-\nabla\cdot\overline{\mathbf{J}_\mathbf{S}} - D_e\frac{\mathbf{S}}{\lambda_{sf}^2} - \mathbf{T}_\mathbf{S} = \mathbf{0}, \tag{4b}$$

where μ_B is the Bohr magneton, e is the electron charge, β_σ and β_D are polarization parameters, λ_{sf} is the spin-flip length, $\otimes$ is the outer product, and $\mathbf{T}_\mathbf{S}$ is defined in (3). $\mathbf{J}_\mathbf{C}$ is the charge current density, $\overline{\mathbf{J}_\mathbf{S}}$ is the spin current tensor, where the components $J_{S,ij}$ indicate the flow of the i-th component of spin polarization in the j-th direction, $\nabla\cdot\overline{\mathbf{J}_\mathbf{S}}$ is the divergence of $\overline{\mathbf{J}_\mathbf{S}}$ with components $\left(\nabla\cdot\overline{\mathbf{J}_\mathbf{S}}\right)_i = \sum_j \frac{\partial J_{S,ij}}{\partial x_j}$, and $\nabla\mathbf{S}$ is the vector gradient of $\mathbf{S}$, with components $(\nabla\mathbf{S})_{ij} = \frac{\partial S_i}{\partial x_j}$. The term $(\nabla\mathbf{S})^T\mathbf{m}$ is a vector with components $\left((\nabla\mathbf{S})^T\mathbf{m}\right)_i = \sum_j \frac{\partial S_j}{\partial x_i} m_j$.

The computation of the spin accumulation permits to straightforwardly describe the magnetization dynamics of complex, multi-layered systems, such as modern MRAM devices. The task of solving the equations for the spin accumulation in such an environment can be well handled by employing the FE Method. We used the open library MFEM [13] to build an in–house solver for the spin accumulation. The FE formulation employed is taken after [11], and is reported in the Appendix.

In order to test our solver, we used the analytical solution reported in [17] to compute the spin accumulation and spin torques in the FL, magnetized along the z-direction, with a fully spin-polarized current coming from the left interface at x = 0 nm. Such a current could be generated by a half metallic thick RL in a spin-valve. The magnetization in the RL is $\mathbf{m} = cos\theta \mathbf{e}_z - sin\theta \mathbf{e}_y$. For this simulation, the term containing λ_φ is not considered, and a fixed current $J_C = 10^{11}$ A/m^2 in the x-direction is applied. The parameters employed in the simulation are reported in Table 1. In Fig. 2 the analytical solution is compared to the one

Table 1
Parameters used in the simulations.

Parameter	Value
Charge polarization, β_σ	0.9
Spin polarization, β_D	0.8
Electron diffusion coefficient in NM, $D_{e,NM}$	2.0×10^{-3} m^2/s
Electron diffusion coefficient in FL and RL, $D_{e,FM}$	2.0×10^{-3} m^2/s
Spin flip length, λ_{sf}	10 nm
Spin exchange length, λ_J	2 nm
Spin dephasing length, λ_φ	5 nm
Voltage applied, V_0	3.34 V
Middle layer conductivity, σ_0	29.76 S/m
Tunneling magnetoresistance, *TMR*	200 %

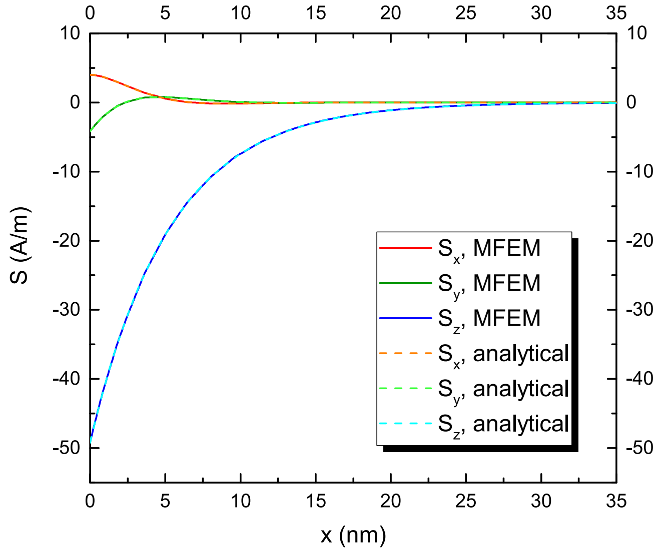

Fig. 2. Comparison between the spin accumulation computed analytically (dotted lines) and using our FE solver (solid lines). The analytical solution [17] is properly reproduced.

computed with our solver. For this kind of simulation, the lateral dimension of the structure does not have any impact on the solution. The expected behavior of the spin accumulation is optimally reproduced by the numerical results.

Eq. (3) for the torque acting on the magnetization comes from the conservation of spin angular momentum. When one neglects spin-flip scattering, the torque can be also computed from the relation

$$\mathbf{T_S} = -\nabla\cdot\overline{\mathbf{J_S}}. \quad (5)$$

These two equations for the computation of the torque should provide compatible results, provided that λ_J and λ_φ are shorter than λ_{sf}, as is the case for spin-valves and MTJs, where the transverse components of the spin accumulation and spin current are absorbed near the interface between the ferromagnetic layer and the middle layer. We computed the torques with both approaches to check the validity of these assumptions. First, the spin current is computed from the spin accumulation solution using (4a), and is reported in Fig. 3. It can be noted, that near the interface the spin current is fully polarized along the direction of the magnetization in the RL. This component is quickly absorbed by the magnetization in the FL. Precession of the spin around the magnetization direction creates a component in the x-direction, perpendicular to the common plane of the magnetization vectors in the RL and the FL. This component is also absorbed on the length scale dictated by λ_J. The spin current gets then polarized in the direction of the magnetization in the FL.

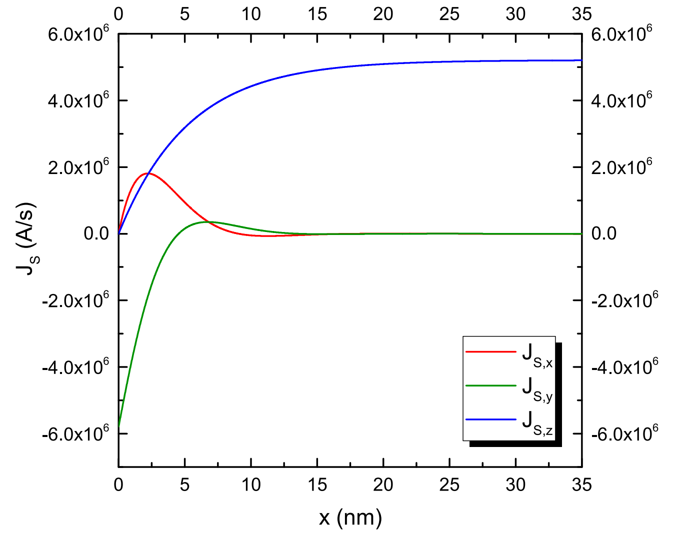

Fig. 3. Spin current computed from the spin accumulation in Fig. 2. The orthogonal components get absorbed near the interface, and the spin current gets polarized along the magnetization direction.

The comparison of the torques computed using (3) and (5) is reported in Fig. 4, where the former is labeled as $\mathbf{T_1}$, while the latter is labeled as $\mathbf{T_2}$. The adiabatic component of the torque is the one lying in the plane formed by the magnetization vectors in the RL and the FL, and tends to align them in the parallel or anti-parallel configuration, depending on the sign of the electric current. The non-adiabatic component is perpendicular to the plane, and creates precession in a field-like manner. The torques computed from both methods are in very good agreement, justifying the use of (5) for computing the torques directly from the spin current.

After testing the accuracy of the finite element implementation in computing the spin accumulation and torques, we can employ it to describe the magnetization dynamics of a multi-layered structure. The spin and charge drift–diffusion formalism has been already successfully applied to the computation of the torques acting in a spin-valve structure with a metallic spacer layer [11,12,19]. However, the cell of an STT-MRAM is composed of a magnetic tunnel junction. It is then necessary to find a way to incorporate the tunnel junction properties when solving the drift–diffusion equations.

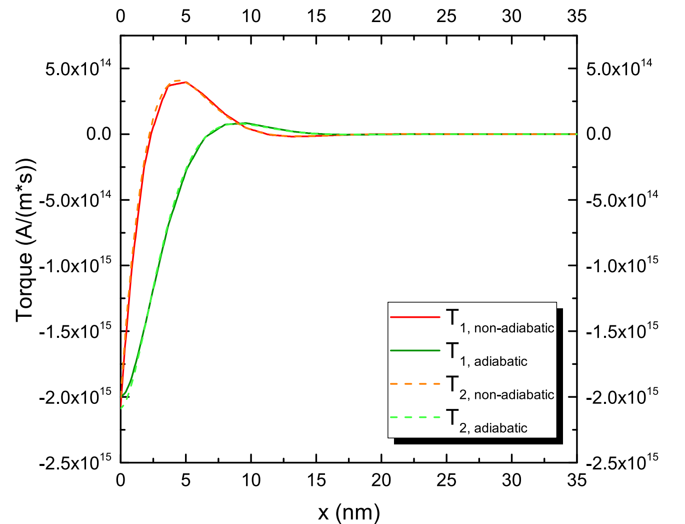

Fig. 4. Comparison between the torque computed using (3) ($\mathbf{T_1}$) and (5) ($\mathbf{T_2}$). The results are in very good agreement and justify the use of (5) for computing the torques.

4. MTJ model

The main feature of an MTJ is the strong dependence of the resistance of the structure on the relative magnetization orientation in the free and reference layers. The amount of current flowing through the structure is also mainly determined by the tunneling resistance, as it is much larger than the resistances of the ferromagnetic layers. In order to reproduce these properties, as we are not interested in their precise physical origin, we model the oxide layer as a poor conductor whose low conductivity depends on the relative magnetization vectors orientation as [10,20]

$$\sigma(\theta) = \sigma_0\left(1 + \left(\frac{TMR}{2+TMR}\right)\cos\theta\right), \tag{6}$$

where σ_0 is the average between the conductivities in the P and AP state, and θ is the local angle between the magnetic vectors in the free and reference layer. With this approach, we want to capture the fact that, in a micromagnetic scenario, the current flowing at a particular point can be position dependent, and that the difference between the parallel and anti-parallel values of the conductance of the structure depends on the TMR. We also obtain a voltage drop localized mainly in the middle layer, while the effects of spin on the electrical voltage and current are included in the second term of (4a). To obtain the current, we solve

$$\nabla\cdot(\sigma(\theta)\nabla V) = 0, \tag{7a}$$

$$\mathbf{J_C} = \sigma(\theta)\nabla V, \tag{7b}$$

where σ is the conductivity, V is the electrical potential and $\mathbf{J_C}$ is the current density. In the FE setting, the angle θ is computed as follows: for every point of the middle layer, a point with the same y- and z-coordinate and the closest x-coordinate is found for both, the free and the reference layer. The scalar product of the magnetization vectors in these two points is computed to obtain the cosine of the angle between them. The equation is solved in the structure schematized in Fig. 1. The magnetization distribution is taken to be parallel in the center of the structure, and anti-parallel on the sides, to showcase the possible range of variation of the current density. The potential is fixed with Dirichlet conditions on the left and right boundaries. The conductivity is constant in the ferromagnetic layers and in the non-magnetic leads, while it is described by (6) in the tunneling layer. For non-uniform magnetization, characteristic to switching, the conductivity in an MTJ depends strongly on the position. The current density solution for this scenario is computed via the FE Method and is reported in Fig. 5. The resulting current flowing through the structure is highly non-uniform, with the difference between highest and lowest values of its perpendicular component determined by the high TMR, which was not previously addressed in the drift–diffusion FE formulation [11,19]. The absolute values of the in-plane current density are redistributed in order to accommodate for the varying conductivity in the middle layer. Once the current density $\mathbf{J_C}$ is known, the spin current density $\mathbf{J_S}$ and the spin accumulation $\mathbf{S}$ are computed using (4). The torques can then be obtained through (3), and are displayed in Fig. 6 for the parameters of Table 1.

We then investigate the dependence of the torques on the parameters entering Eq. (4), in order to calibrate our model and to understand, if realistic parameters reproduce the STT torque predicted by Slonczewski [10]. We set the magnetization in the RL pointing in the x-direction, and the magnetization in the FL pointing in the z-direction. We use the structure depicted in Fig. 1, with ferromagnetic layers of 2 nm thickness, a middle layer of 1 nm thickness, and non-magnetic leads of 30 nm thickness. In Fig. 7, the dependencies on different system parameters are reported. The non-varying parameters are taken from Table 1, unless differently stated. We note that, when solving (4) with the FE approach, the simulation domain is bounded with homogeneous Neumann

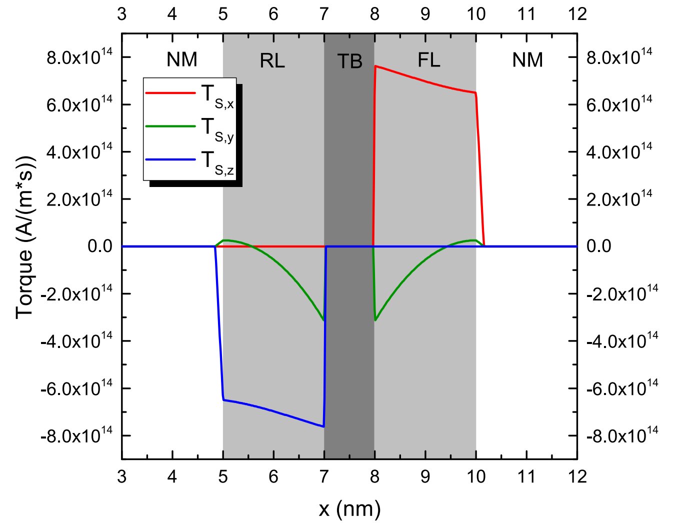

Fig. 6. Torque computed from the spin accumulation, with the magnetization in the RL pointing in the x-direction and the one in the FL pointing in the z-direction. The spin drift–diffusion approach permits to compute the torques acting on both layers, FL and RL.

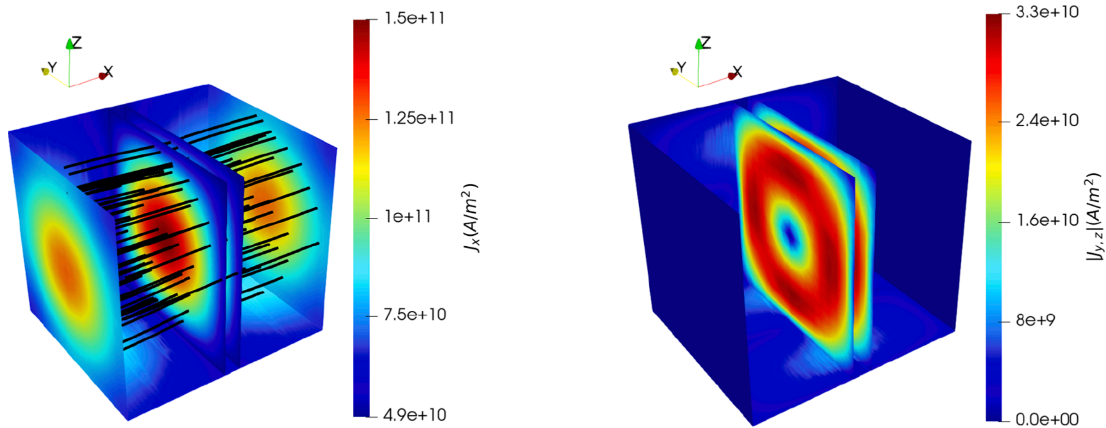

Fig. 5. Current density distribution through a square MTJ with a non-uniform magnetization. The left panel shows the x-component (perpendicular) of the current density, with black lines representing the streamlines of the current density vector field, while the right panel shows the modulus of the y- and z- (in-plane) components. The x-component flow is higher for aligned magnetizations because of the lower resistance. Due to conservation of the current flow, it is redistributed in the yz-plane in the metal contacts.

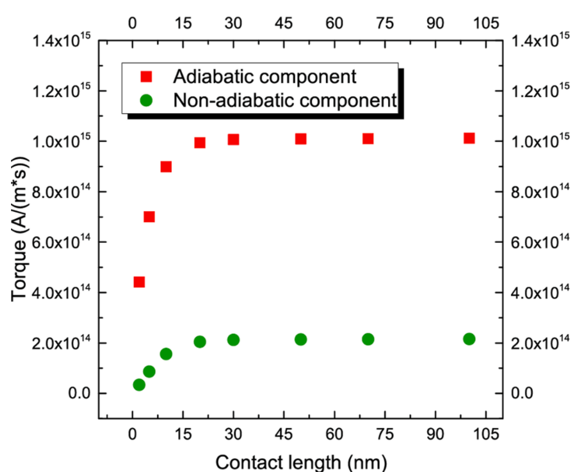

(a)

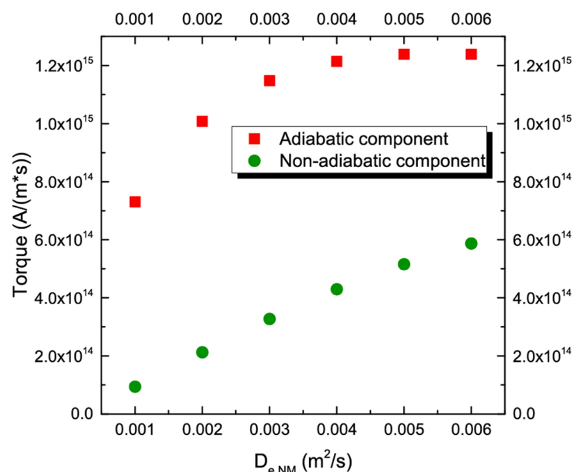

(b)

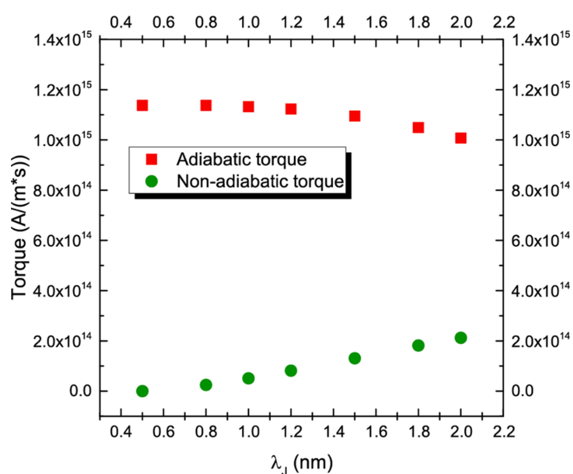

(c)

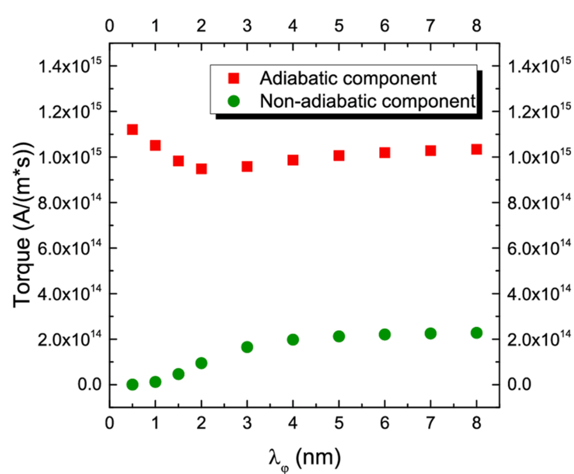

(d)

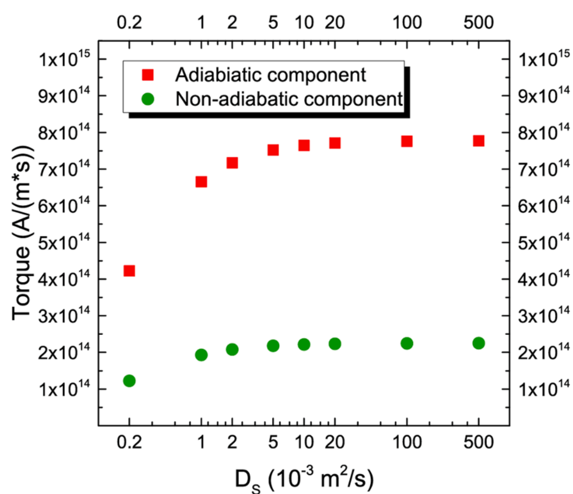

(e)

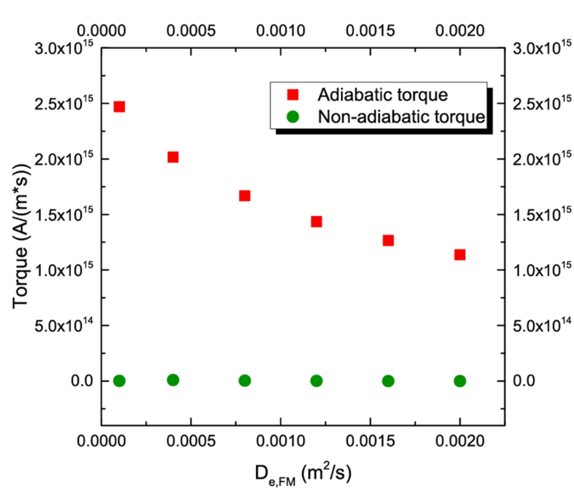

(f)

Fig. 7. Dependence of the average torques acting on the free layer on various system parameters. Details are reported in the main text.

conditions, $\frac{\partial \mathbf{S}}{\partial \mathbf{n}} = \mathbf{0}$. This can lead to a non-physical behavior, if the contacts included in the model are not long enough to allow spin accumulation and current to relax to zero [12,19]. Fig. 7(a) reports the dependence on the length of the non-magnetic contacts. For our choice of parameters, a contact thickness of at least 30 nm is required to let **S** decay to **0** and obtain a torque value independent of the contacts' lengths. Fig. 7(b) reports the dependence on the magnitude of the diffusion coefficient in the non-magnetic contacts, showing that, even if the exchange between the magnetization and the spin accumulation happens in the ferromagnetic layers, this parameter still has an effect on the torque magnitude, due to the continuous nature of the spin accumulation in the FE setting. Fig. 7(c) then reports the dependence on the value of the exchange length. Lower values of λ_J imply a stronger exchange coupling, and produce an increased adiabatic torque. They also change the relative importance of the non-adiabatic component coming from the drift–diffusion formalism. A shorter λ_J also implies a faster absorption of the transverse components of **S**, so that values below 1 nm bring these components to almost 0 in the space of the FL. We also investigated the influence of the usually neglected [11,17] spin dephasing length λ_φ on the computation of the torque. Results are reported in Fig. 7(d). For values of λ_φ less than 3 nm, its contribution to the torque is substantial. This suggests that, when the value of λ_φ is close to λ_J, the effects of the former has to be taken into consideration for accurately describing the magnetization dynamics. In Fig. 7(e) we show the dependence on the diffusion parameter in the middle layer, labeled D_S. In this layer, where $\mathbf{m} = \mathbf{0}$, Eq. (4b) reduces to

$$D_S \nabla^2 \mathbf{S} - D_S \frac{\mathbf{S}}{\lambda_{sf}^2} = \mathbf{0}. \tag{8}$$

The spin-flip length is assumed infinite inside the barrier. The value of D_S can then be used as an additional tuning parameter for the torques. The results reported in the figure show that the torques increase with the diffusion coefficient, becoming constant at a value $D_S = 2.5 \times 10^{-1}$ m^2/s, which is the one employed for the simulations reported in this paper. For this value of D_S, the slope of **S** in the middle layer is reduced to the point where the spin accumulation is practically preserved from the RL to the FL. Finally, Fig. 7(f) reports the dependence of the torque on the diffusion coefficient of the ferromagnetic layers. For this plot, we employed an exchange length $\lambda_J = 0.5$ nm, which lets the torques be entirely absorbed in the ferromagnetic layers. The results show that a lower value of $D_{e,FM}$ increases the magnitude of the adiabatic torque, as the first term in Eq. (4a), describing the magnetization dependent polarization of the electric current, becomes dominant over diffusive effects.

The adiabatic torque acting on the FL of an MTJ predicted by Slonczewski [10] is of the form

$$\mathbf{T_S} = -\frac{g\mu_B P_{RL} J_C}{2ed(1 + P_{FL}P_{RL}\cos\theta)}(\mathbf{m_{FL}} \times (\mathbf{m_{FL}} \times \mathbf{m_{RL}})), \tag{9}$$

where g is the g-factor, $P_{FL}, P_{RL}, \mathbf{m_{FL}}$ and $\mathbf{m_{RL}}$ are the polarizing factors and magnetization vectors of the FL and RL, respectively, d is the thickness of the FL, and θ is the angle between the magnetization vectors. With $\theta = 90^\circ$ and $P_{RL} = P_{FL} = 0.7$, this produces a torque in the FL of $|\mathbf{T_S}| = 2.03 \cdot 10^{15} \frac{A}{ms}$. We can use the previous analysis to calibrate the torque produced by our solver on the one predicted by Slonczewski. In Fig. 8 we report the spin accumulation solution for the modified set of parameters reported in Table 2. The lower exchange length allows the transverse components of **S** to be completely absorbed inside the FL, while the lower value of the diffusion coefficient in the ferromagnetic layers can be justified by a lower conductivity value of CoFeB when compared to normal metals [21]. The torque acting on both ferromagnetic layers is reported in Fig. 9. By integrating the x-component of this torque over the whole free layer, we obtain a value of $|\mathbf{T_S}| = 2.02 \cdot 10^{15}$ $\frac{A}{ms}$, which is compatible with the value computed using (9). Fig. 10 shows the dependence of the average torque acting on both the FL and RL, as computed by the FE solver, on the polarization parameter of the RL, $\beta_{\sigma,RL}$. The torque on the FL shows a linear dependence on this parameter, while the torque on the RL is almost independent of it. This behavior is compatible with the dependence on P_{RL} expected from (9).

Finally, we show a solution for the spin accumulation, computed

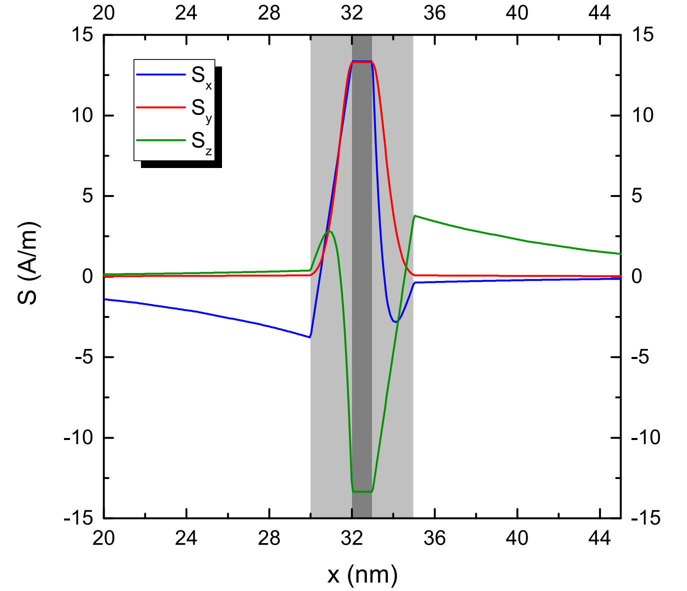

Fig. 8. Spin accumulation computed with the modified parameters reported in Table 2. The transverse components of the spin accumulation get absorbed inside the free layer.

Table 2
Modified parameters used to reproduce the Slonczewski torque magnitude.

Parameter	Value
Charge polarization, β_σ	0.7
Electron diffusion coefficient in NM, $D_{e,NM}$	1.0×10^{-2} m^2/s
Electron diffusion coefficient in FL and RL, $D_{e,FM}$	1.0×10^{-4} m^2/s
Spin exchange length, λ_J	0.5 nm

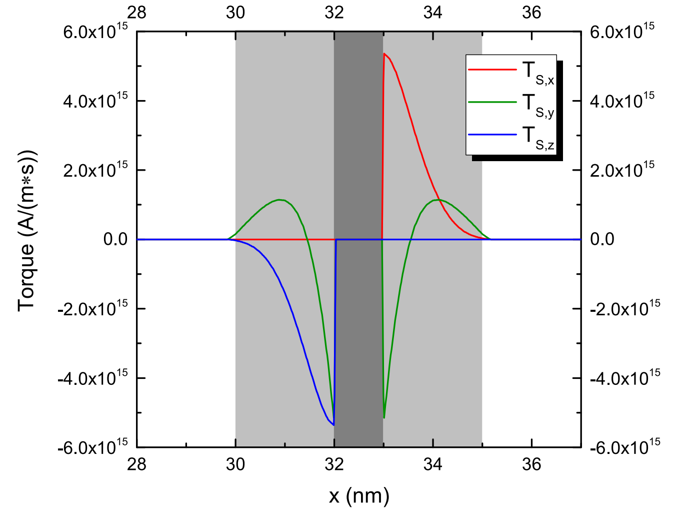

Fig. 9. Torque computed with the parameters reported in Table 2. The average value of the adiabatic torque is compatible with what predicted by Slonczewski for an MTJ.

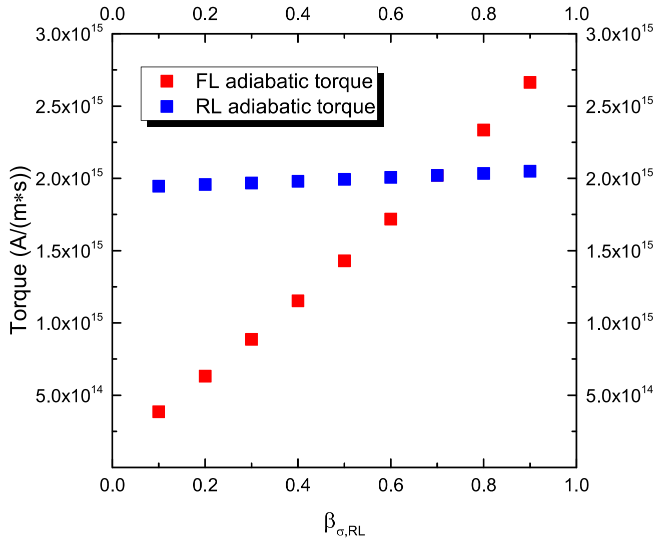

Fig. 10. Dependence of the average torque acting on the FL and RL on the polarization parameter of the RL, $\beta_{\sigma,RL}$.

using the parameters in Table 2, with the non-uniform magnetization configuration reported in Fig. 1 and the electrical current reported in Fig. 5. The results for the three components of **S** are reported in Fig. 11. The spin accumulation is redistributed, in both layers, in response to both the magnetization configuration and the current density distribution. This solution, computed using (4), (6) and (7), can be employed for computing the torque (3) acting in (2) and calculating the magnetization dynamics.

These results show that we compute the spin accumulation with the right sign and magnitude to reproduce typical values of the STT torque expected in an MTJ. The FE approach to the drift–diffusion formalism gives the possibility of computing the torques in all the ferromagnetic layers of the structure for a variety of three-dimensional meshes. We note, however, that the torques computed by our approach pose a strictly linear dependence on the bias voltage, coming from the first term of Eq. (4a) and from the linear dependence of J_C on V from Eq. (7). Theoretical calculations employing the non-equilibrium Green function technique (NEGF) [22,23] have shown that, at high bias voltage, the adiabatic component shows a nonlinear behavior, while the non-adiabatic component has a symmetric and quadratic dependence. A possible way of solving these limitations of our approach is to lift the constraint of the continuity of **S** at the tunneling interface, and to employ boundary conditions to include the spin polarization effects of the barrier itself, which is beyond the scope of the presented investigations and

Fig. 11. Spin accumulation computed with non-uniform magnetization configuration. The top left panel reports the x-component, the top-right panel reports the y-component, and the bottom panel reports the z-component. The values are reported for 4 planes, located in the middle of the RL, at the left interface of the TB, at the right interface of the TB and in the middle of the FL, respectively.

results.

5. Conclusion

We tested a Finite Element implementation of a setup for the solution of the spin drift–diffusion equations against known analytical results which where adequately reproduced. We then showed a method of applying the same spin drift–diffusion simulation approach to an MTJ structure. The current can be successfully simulated by modeling the tunnel barrier as a poor conductor with an electrical conductivity locally depending on the relative magnetization orientation in the ferromagnetic layers. We then investigated the dependence of the torque magnitude on various parameters entering the drift–diffusion formalism, such as the exchange and spin-dephasing lengths, the diffusion coefficient of the ferromagnetic, non-magnetic and tunneling layers, and the length of the contacts. We showed that, with a proper set of parameters, the spin torque magnitude matches the one expected in an MTJ structure. Our generalized spin and charge drift–diffusion approach can be successfully applied to determine the torques acting on the magnetization in modern STT-MRAM devices.

Declaration of Competing Interest

The authors declare that they have no known competing financial interests or personal relationships that could have appeared to influence the work reported in this paper.

Acknowledgment

The financial support by the Austrian Federal Ministry for Digital and Economic Affairs and the National Foundation for Research, Technology and Development is gratefully acknowledged.

Appendix

The weak formulation of Eq. (4b) employed by the FE solver is

$$D_e\int_\Omega \nabla\mathbf{S}:\nabla\mathbf{v}\,d\mathbf{x} - D_e\beta_\sigma\beta_D\int_\Omega\left[\mathbf{m}\otimes\left((\nabla\mathbf{S})^{\mathrm{T}}\mathbf{m}\right)\right]:\nabla\mathbf{v}\,d\mathbf{x} + \frac{D_e}{\lambda_{sf}^2}\int_\Omega \mathbf{S}\cdot\mathbf{v}\,d\mathbf{x} + \frac{D_e}{\lambda_J^2}\int_\Omega(\mathbf{S}\times\mathbf{m})\cdot\mathbf{v}\,d\mathbf{x} + \frac{D_e}{\lambda_\varphi^2}\int_\Omega(\mathbf{m}\times(\mathbf{S}\times\mathbf{m}))\cdot\mathbf{v}\,d\mathbf{x} = \frac{\mu_B}{e}\beta_\sigma\int_\omega[\mathbf{m}\otimes\mathbf{J_e}] :\nabla\mathbf{v}\,d\mathbf{x} - \frac{\mu_B}{e}\beta_\sigma\int_{\partial\Omega\cap\partial\omega}(\mathbf{J_e}\cdot\mathbf{n})(\mathbf{m}\cdot\mathbf{v})\,d\mathbf{x} \tag{10}$$

where $\mathbf{v}$ is a vector test function, Ω is the whole volume of the structure, ω is the volume of the magnetized regions, and $\mathbf{n}$ is the boundary outer normal. $\nabla\mathbf{a}:\nabla\mathbf{b} = \sum_{ij}(\nabla\mathbf{a})_{ij}(\nabla\mathbf{b})_{ij}$ is the Frobenius inner product of two matrices. Such a formulation produces continuity of both $\mathbf{S}$ and $\overline{\mathbf{J_S}}\,\mathbf{n}$ at internal interfaces, while the condition $\frac{\partial\mathbf{S}}{\partial\mathbf{n}} = \mathbf{0}$ is assumed for external boundaries.

The weak formulation of Eq. (7a) is

$$\int_\Omega \sigma(\theta)\nabla V\cdot\nabla v\,d\mathbf{x} = 0 \tag{11}$$

with voltage fixed with Dirichlet conditions at the left and right boundaries of the structure. v is a scalar test function.

References

[1] Hanyu T, Endoh T, Suzuki D, Koike H, Ma Y, Onizawa N, et al. Standby-power-free integrated circuits using MTJ-based VLSI computing. Proc IEEE 2016;104:1844–63. https://doi.org/10.1109/JPROC.2016.2574939.
[2] Gallagher WJ, Chien E, Chiang T, Huang J, Shih M, Wang CY, et al. 22 nm STT-MRAM for reflow and automotive uses with high yield, reliability, and magnetic immunity and with performance and shielding options. In: Proc IEDM Conf 2019: 2.7.1–2.7.4. https://doi.org/10.1109/IEDM19573.2019.8993469.
[3] Sakhare S, Perumkunnil M, Bao TH, Rao S, Kim W, Crotti D, et al. Enablement of STT-MRAM as last level cache for the high performance computing domain at the 5nm node. In: Proc IEDM Conf 2018:18.3.1–18.3.4. https://doi.org/10.1109/IEDM.2018.8614637.
[4] Aggarwal S, Almasi H, DeHerrera M, Hughes B, Ikegawa S, Janesky J, Lee HK, et al. Demonstration of a reliable 1 Gb standalone spin-transfer torque MRAM for industrial applications. In: Proc IEDM Conf 2019:2.1.1–2.1.4. https://doi.org/10.1109/IEDM19573.2019.8993516.
[5] Lee K, Bak JH, Kim YJ, Kim CK, Antonyan A, Chang DH, et al. 1 Gbit high density embedded STT-MRAM in 28nm FDSOI technology. In: Proc IEDM Conf 2019: 2.2.1–2.2.4. https://doi.org/10.1109/IEDM19573.2019.8993551.
[6] Naik VB, Lee K, Yamane K, Chao R, Kwon J, Thiyagarajah N, et al. Manufacturable 22nm FD-SOI embedded MRAM technology for industrial-grade MCU and IOT applications. In: Proc IEDM Conf; 2019. p. 2.3.1–4. https://doi.org/10.1109/IEDM19573.2019.8993454.
[7] Alzate JG, Arslan U, Bai P, Brockman J, Chen YJ, Das N, et al. 2 Mb array-level demonstration of STT-MRAM process and performance towards L4 cache applications. In: Proc IEDM Conf; 2019. p. 2.4.1–4. https://doi.org/10.1109/IEDM19573.2019.8993474.
[8] Hu G, Nowak JJ, Gottwald MG, Brown SL, Doris B, D'Emic CP, et al. Spin-transfer torque MRAM with reliable 2 ns writing for last level cache applications. In: Proc IEDM Conf; 2019. p. 2.6.1–2.6.4. https://doi.org/10.1109/IEDM19573.2019.8993604.
[9] Slonczewski JC. Current-driven excitation of magnetic multilayers. J Magn Magn Mater 1996;159:L1–7. https://doi.org/10.1016/0304-8853(96)00062-5.
[10] Slonczewski JC. Currents, torques, and polarization factors in magnetic tunnel junctions. Phys Rev B 2005;71:024411. https://doi.org/10.1103/PhysRevB.71.024411.
[11] Abert C, Ruggeri M, Bruckner F, Vogler C, Hrkac G, Praetorius D, et al. A three-dimensional spin-diffusion model for micromagnetics. Sci Rep 2015;5:14855. https://doi.org/10.1038/srep14855.
[12] Lepadatu S. Unified treatment of spin torques using a coupled magnetisation dynamics and three-dimensional spin current solver. Sci Rep 2017;7:12937. https://doi.org/10.1038/s41598-017-13181-x.
[13] Anderson R, Andrej J, Barker A, Bramwell J, Camier J-S, Cerveny J, et al. MFEM: A modular finite element library. Comput Math Appl 2020;81:42–74. https://doi.org/10.1016/j.camwa.2020.06.009.
[14] Fiorentini S, Ender J, Selberherr S, de Orio RL, Goes W, Sverdlov V. Comprehensive modeling of coupled spin and charge transport through magnetic tunnel junctions. In: Proc EUROSOI-ULIS Conf; 2020. p. 1–4. https://doi.org/10.1109/EUROSOI-ULIS49407.2020.9365497.
[15] Skowroński W, Czapkiewicz M, Zietek S, Chęciński J, Frankowski M, Rzeszut P, et al. Understanding stability diagram of perpendicular magnetic tunnel junctions. Sci Rep 2017;7:10172. https://doi.org/10.1038/s41598-017-10706-2.
[16] Bhatti S, Sbiaa R, Hirohata A, Ohno H, Fukami S, Piramanayagam S. Spintronics based random access memory: a review. Mater Today 2017;20:530–48. https://doi.org/10.1016/j.mattod.2017.07.007.
[17] Zhang S, Levy PM, Fert A. Mechanisms of spin-polarized current-driven magnetization switching. Phys Rev Lett 2002;88:236601. https://doi.org/10.1103/PhysRevLett.88.236601.
[18] Fiorentini S, de Orio RL, Goes W, Ender J, Sverdlov V. Comprehensive comparison of switching models for perpendicular spin-transfer torque MRAM cells. In: Proc IEDM Conf 2019:1–4. https://doi.org/10.1109/SISPAD.2019.8870359.
[19] Abert C, Ruggeri M, Bruckner F, Vogler C, Manchon A, Praetorius D, et al. A self-consistent spin-diffusion model for micromagnetics. Sci Rep 2016;6:16. https://doi.org/10.1038/s41598-016-0019-y.
[20] Zhu J-G, Park C. Magnetic tunnel junctions. Mater Today 2006;9:36–45. https://doi.org/10.1016/S1369-7021(06)71693-5.

[21] Jen SU, Yao YD, Chen YT, Wu JM, Lee CC, Tsai TL, et al. Magnetic and electrical properties of amorphous CoFeB films. J Appl Phys 2006;99:053701. https://doi.org/10.1063/1.2174113.
[22] Chshiev M, Manchon A, Kalitsov A, Ryzhanova N, Vedyayev A, Strelkov N, et al. Analytical description of ballistic spin currents and torques in magnetic tunnel junctions. Phys Rev B 2015;92:104422. https://doi.org/10.1103/PhysRevB.92.104422.
[23] Camsari KY, Ganguly S, Datta D, Datta S. Physics-based factorization of magnetic tunnel junctions for modeling and circuit simulation. In: Proc IEDM Conf; 2014. p. 35.6.1–4. https://doi.org/10.1109/IEDM.2014.7047177.

Simone Fiorentini was born 1992 in Verona, Italy. He received his Bachelor degree and Master Degree in Physics from the University of Padova, in 2014 and 2017, respectively. He carried out his Master Thesis at the Ruprecht-Karls University of Heidelberg through the Erasmus Program. After a short period working for an IT company in Milan, Italy, he joined the Institute for Microelectronics in November 2018, where he started his PhD studies. He is currently investigating ways to appropriately simulate both spin and magnetization dynamics in magnetoresistive memories, in the scope of the Christian Doppler Laboratory on Nonvolatile Magnetoresistive Memory and Logic.